



The teleseismic signature of fossil subduction: Northwestern Canada

J.-P. Mercier,¹ M. G. Bostock,¹ P. Audet,¹ J. B. Gaherty,² E. J. Garnero,³
and J. Revenaugh⁴

Received 20 April 2007; revised 22 November 2007; accepted 18 January 2008; published 29 April 2008.

[1] Between June 2003 and September 2005, 20 broadband, three-component seismometers were deployed along the MacKenzie-Liard Highway in Canada's Northwest Territories as part of the joint Lithoprobe-IRIS Canada Northwest Experiment (CANOE). These stations traverse a paleo-Proterozoic suture and subduction zone that has been previously documented to mantle depths using seismic reflection profiling. Teleseismic receiver functions computed from ~250 earthquakes clearly reveal the response of the ancient subduction zone. On the radial component, the suture is evident as a direct conversion from the Moho, the depth of which increases from ~30 km to ~50 km over a horizontal distance of ~70 km before its signature disappears. The structure is still better defined on the transverse component where the Moho appears as the upper boundary of a 10 km thick layer of anisotropy that can be traced from 30 km to at least 90 km depth. The seismic response of this layer is characterized by a frequency dependence that can be modeled by upper and lower boundaries that are discontinuous in material properties and their gradients, respectively. Anisotropy can be characterized by a $\pm 5\%$ variation in shear velocity and hexagonal symmetry with a fast axis that plunges at an oblique angle to the subduction plane. The identification of this structure provides an unambiguous connection between fossil subduction and fine-scale, anisotropic mantle layering. Previous documentation of similar layering below the adjacent Slave province and from a range of Precambrian terranes across the globe provides strong support for the thesis that early cratonic blocks were stabilized through processes of shallow subduction.

Citation: Mercier, J.-P., M. G. Bostock, P. Audet, J. B. Gaherty, E. J. Garnero, and J. Revenaugh (2008), The teleseismic signature of fossil subduction: Northwestern Canada, *J. Geophys. Res.*, 113, B04308, doi:10.1029/2007JB005127.

1. Introduction

[2] Northwestern Canada is composed of a variety of geological terranes that formed and accreted over the past 4.0 Ga. This unique collage spans over 5000 km from the Pacific coast in the west to the Slave craton in the east, and represents the most nearly complete and contiguous sampling of geological time on the surface of the Earth. Consequently, the region is particularly well suited to address fundamental questions concerning the nature of continental evolution and variations in structure and geometry of the subsurface from early Archean (3.5–4.0 Ga) to present.

[3] In the 1990s, the Lithoprobe Slave-Northern Cordillera Lithospheric Evolution transect, hereafter referred to as SNORCLE, was undertaken over this region [Cook and

Erdmer, 2005]. It comprised a series of geophysical and geological experiments that led to several important discoveries. In particular, an active-source, seismic reflection experiment in the Wopmay orogen revealed the presence of several clearly defined and laterally coherent mantle reflectors [Cook *et al.*, 1998, 1999]. The most prominent among them is an eastward dipping layer in the lithospheric mantle merging with the crust at the suture of Fort Simpson and Hottah terranes, and extending eastward beneath the Great Bear magmatic arc where it reaches a depth of ~100 km (see Figure 1b for geographic location). Geological and geophysical evidence indicates that this feature is a remnant of Proterozoic subduction. Although several other similar reflectors were observed further east toward and below the Slave province, their relation with the dipping structure described above has remained unclear.

[4] Also beneath the Slave province, a teleseismic-*P* receiver function study by Bostock [1998] using data recorded at the Yellowknife (YKA) medium-aperture seismic array shows a well developed mantle stratigraphy. Three major layered structures, defined by discontinuous boundaries between azimuthally anisotropic domains, were identified, and labeled *H*, *X* and *L* at depths of 75, 135, and 170 km, respectively. Labels *H* and *L* are used generically to

¹Department of Earth and Ocean Sciences, The University of British Columbia, Vancouver, British Columbia, Canada.

²Lamont-Doherty Earth Observatory, Palisade, New York, USA.

³School of Earth and Space Exploration, Arizona State University, Tempe, Arizona, USA.

⁴Department of Geology and Geophysics, University of Minnesota, Minneapolis, Minnesota, USA.

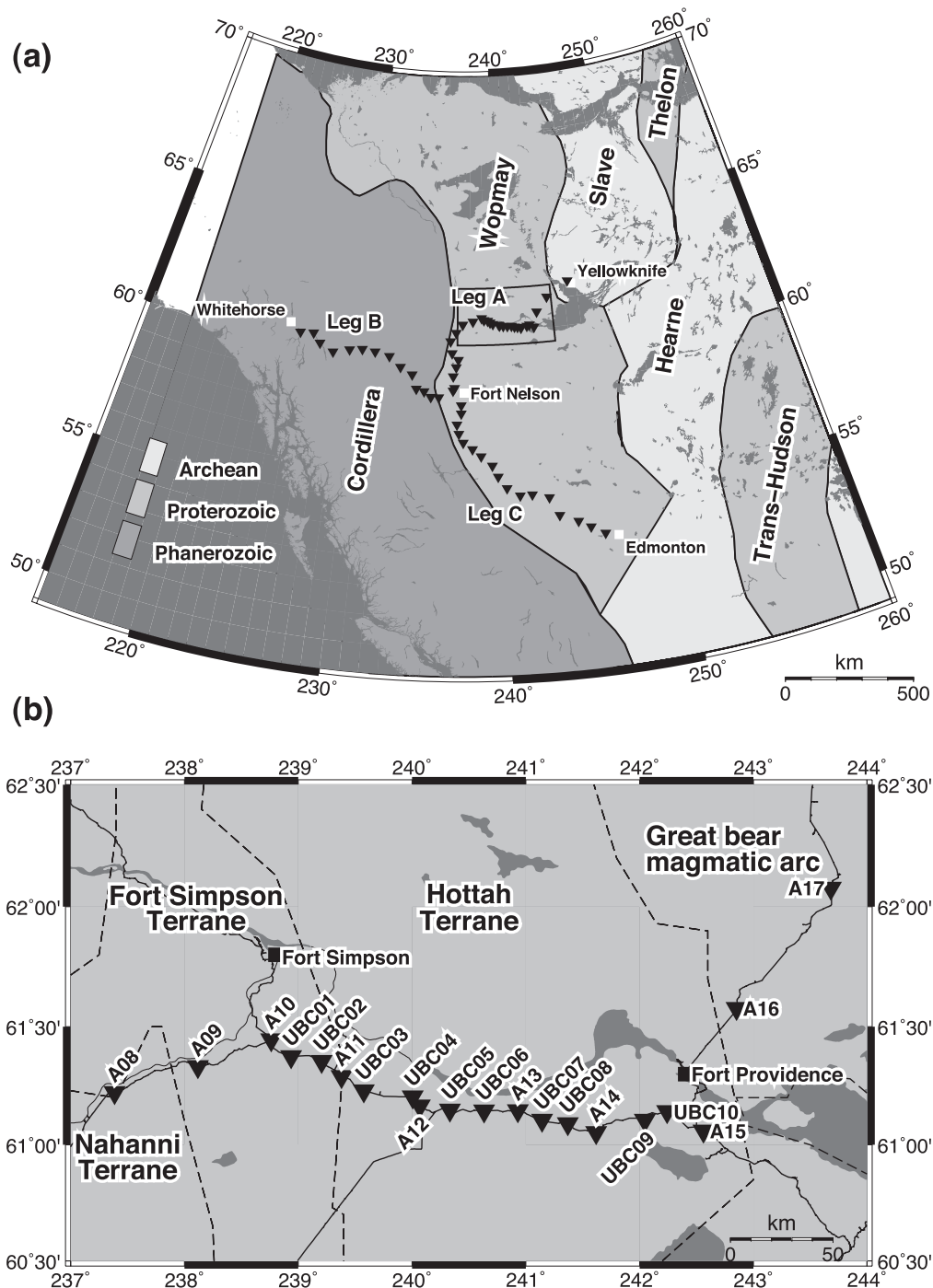


Figure 1. (a) Map of western Canadian geological provinces illustrating the distribution of the broadband three-component CANOE stations along legs A, B and C. The three legs radiate away from Fort Nelson to Yellowknife (leg A), Whitehorse (leg B) and Edmonton (leg C). The study area is identified by the inset portion of leg A. (b) Inset of study region where 20 broadband three-component seismic stations were deployed at ~35 km intervals at the ends and ~15 km intervals in the center. The dashed lines delineate different geological terranes within the Wopmay Orogen.

represent the so-called Hales and Lehman discontinuities, see also, e.g., *Revenaugh and Jordan [1991]* and *Gaherty and Jordan [1995]*. The structures beneath the Slave craton were hypothesized to represent stranded, former oceanic crustal material emplaced during a series of subduction episodes. This discovery prompted speculation on a possible

continuation of the dipping layer, defined on the SNORCLE reflection profile, eastward beneath the Slave province, and on the importance of subduction processes in the formation and stabilization of the underlying cratonic root.

[5] Our study presents teleseismic receiver-function images of the mantle below the Wopmay orogen from 20

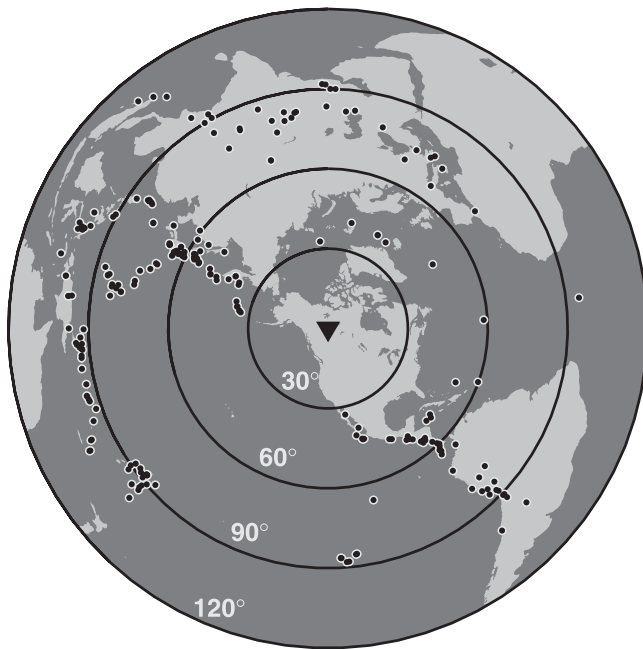


Figure 2. Equidistant azimuthal projection centered on station UBC06 showing the distribution of events recorded over the period 2003–2005 with sufficiently high signal-to-noise ratio at one or more stations of the array to be used in this study. Note the relatively uniform azimuthal sampling between back-azimuth of 225° and 40° (events mainly from Pacific ring of fire, Asia, middle east and Northern Africa), and between 125° to 175° (events mainly from the Americas).

three-component, broadband seismic stations installed in the Northwest Territories as part of the joint Incorporated Research Institutions for Seismology (IRIS)-Lithoprobe CANadian NOorthwest Experiment (hereafter referred to as CANOE) which complements the earlier SNORCLE near-vertical reflection [Cook *et al.*, 1998] and refraction/wide-angle reflection [Fernández-Viejo and Clowes, 2003] profiles. In what follows, we provide further constraints on the nature and geometry of the subsurface structure mentioned above which yield insight into the importance of subduction processes in the stabilization of the Slave craton.

2. Tectonic Setting

[6] The area of interest in this study spans, from west to east, the entire Wopmay orogen complex and the western portion of the Slave province, known as the Anton terrane (see Figure 1b). The Slave province is a relatively small craton that forms, together with the Nain, Superior and Rae provinces, one of the nuclei of the Canadian Shield, the core of the North American continent. It contains the oldest dated rocks on Earth, the Acasta gneiss, estimated at more than 4.03 Ga in age [Bowring and Williams, 1999]. Its assembly was complete by 2.6 Ga, upon the accretion of volcanic arcs and micro-continents [Isachsen and Bowring, 1994].

[7] The formation of Wopmay orogen, a Paleoproterozoic collage of domains, occurred between 2.1 and 1.84 Ga [Hildebrand *et al.*, 1987]. It is composed of three distinct

elements: the Hottah, Fort Simpson and Nahanni terranes. The Hottah terrane developed between 1.92 and 1.91 Ga as a magmatic arc. It collided with the Slave province during the Calderian Orogeny (1.90–1.88 Ga), shortening and displacing the sedimentary rocks of the Coronation margin. Subduction of an oceanic plate beneath the Hottah terrane between 1.88 and 1.84 Ga resulted in formation of the Great Bear magmatic arc located at the eastern edge of the Hottah terrane [Hoffman and Bowring, 1984]. The Fort Simpson terrane accreted to the western margin of Hottah between 1.845 and 1.745 Ga [Villeneuve *et al.*, 1991]. The Nahanni terrane is located west of the Fort Simpson terrane and is the underlying basement to the Northern Cordillera. It reveals no surface exposure and remains an enigmatic geological feature.

3. Data

[8] The CANOE project involved the deployment of an expansive seismic array comprising nearly 60 three-component broadband stations (see Figure 1a). Instrumentation was a mix of Guralp CMG-3T, CMG-ESP, and CMG-40T seismometers and RefTek recorders, provided by various institutions (see Acknowledgments). The array consisted of 3 legs which radiate outward from the array center at Fort Nelson, to Yellowknife (leg A), Whitehorse (leg B) and Edmonton (leg C) spanning more than 3500 km in aperture and traversing an extensive suite of geological domains. The instruments were deployed in June 2003 and 2004 during two separate campaigns and were decommissioned in September 2005 after 27 and 15 months, respectively. The station spacing is on average 35 km over most of the array with the exception of a stretch of Mackenzie Highway between Fort Simpson and Fort Providence on leg A where spacing was reduced to ~ 15 km.

[9] In the present study, we employ a subset of the data from 20 CANOE stations (A08-A17 and UBC01-UBC10) (Figure 1b) traversing the entire Wopmay orogen complex and the western edge of the Slave craton. Over the duration of the experiment teleseismic-*P* waves from ~ 250 earthquakes larger than magnitude 5.5 were recorded in the epicentral distance range 30° – 100° , mainly from the Western Pacific, Fiji-Tonga, Central and South American regions. Consequently, the back-azimuthal coverage is good from 225° to 40° and from 125° to 175° and less regularly sampled otherwise (see Figure 2). Seismogram selection based on signal-to-noise ratio (SNR) (threshold set to 15 dB for the *P*-component seismogram in the 0–2 Hz band) followed by a visual inspection, resulted in a data set that comprises 1428 fair-to-good quality, broadband, three-component recordings with an average of 71 seismograms per station.

4. Methodology

[10] The isolation of scattered S-waves in the teleseismic-*P* coda produced through interaction of the near-vertically propagating incident *P* wave with sub-horizontal discontinuities requires accurate removal of the earthquake source time function. This operation is conventionally performed through a spectral equalization procedure referred to as receiver function analysis [Vinnik, 1977; Langston, 1979]. It consists of accurate decomposition of the incident wave-

field into upgoing P and S modes [e.g., Kennett, 1991] which, when combined with a Wiener spectral deconvolution [Wiener, 1949] of the S -components by the P -component, allows the recovery of an estimate of the S -components (radial and transverse) of the receiver-side Earth's Green's function. The timing of direct P -to- S conversions in the resulting time series depends on the velocity structure and is proportional to the depth of discontinuity whereas their amplitudes scale with the magnitude and sign of the contrasts in elastic moduli and density.

[11] Although a formal 2-D or 3-D inversion for anisotropic parameters is, in principle, possible [Burrige *et al.*, 1998], teleseismic data sets are generally too poorly sampled in slowness and back-azimuth to afford a well-posed inverse problem. We have opted for a simpler imaging scheme that involves the projection of receiver functions to a 2-D profile wherein the amplitudes are color-coded/shaded and displayed as a function of time and horizontal distance. In this way the entire receiver function data set is directly represented and laterally coherent signals, even if weak, are readily apparent.

[12] Receiver functions are ordered from left to right along the resulting profile based on the geographic position of the stations and, for individual stations, on the sampling point of the P - S conversions projected onto the west-east direction (Figure 3a). The station spacing along leg A varies from ~ 45 km (A08–A10 A15–A17) at the ends to ~ 15 km in the center (stations A10 to A15). Differences in station spacing are accounted for by a variable horizontal stretching proportional to the station separation (Figure 3b). This approach allows comparison of the profiles with time-migrated reflection data of Cook *et al.* [1999] through a simple scaling between the direct P -to- S conversion time and the 2-way vertical P reflection time as described in more detail in section 7.

5. Results

[13] Figures 4a and 4b present the raw radial (SV) and transverse (SH) component receiver-function images obtained from the CANOE data. Figure 4c displays a version of the transverse component wherein polarities have been corrected to account for the periodicity of the signal identified as AM . The nature of this correction is described in more detail later in this section. For the sake of comparison with the SNORCLE reflection profile, we have plotted both time and approximate depth axes where, for the latter, we have assumed a Poisson solid with P -velocities of 6 km/s and 8 km/s for crust and mantle, respectively. Note that the assumption of constant Poisson's ratio may not hold along the entire profile [see Fernández-Viejo *et al.*, 2005], but resulting image degradation should be minor given the low frequency content of teleseismic data and the rudimentary imaging scheme. The conversion between delay time Δt_{ps} and depth interval Δz within each layer is thus given by:

$$\Delta z = \frac{V_p \Delta t_{ps}}{\left(\sqrt{3 - V_p^2 p^2} - \sqrt{1 - V_p^2 p^2} \right)}, \quad (1)$$

where p is horizontal slowness and V_p is the P wave velocity. In the following sections we direct our attention to

five prominent and laterally coherent signals labeled S , TM , AM , $A1$, and $A2$.

[14] Signal S is defined on the radial component by a succession of strong positive (red) and negative (blue) pulses within the first 2 s along most of the array, with the exception of stations A16 and A17. Since the occurrence of signal S coincides with the presence of a shallow ~ 1 km thick layer of Phanerozoic sediments that extends from the western limit of our array to the vicinity of Fort Providence (see Figure 1b), it likely represents free-surface reverberations from this structure. The relatively large pulse amplitudes and duration preclude structural investigation of the crust to a depth of ~ 15 km.

[15] On the same component, a clear positive (red) pulse labeled TM (Teleseismic Moho) is visible at around 4 s (~ 30 km) beneath station A08 at the western end of the profile, and corresponds to the P -to- S conversion from the crust-mantle boundary (Moho). It shifts to later times beneath station A09 to ~ 4.5 s, and is relatively constant in time along the rest of the profile with the exception of a 75 km long disruption beginning near kilometer 125. At this point, the signal appears to dip eastward into the mantle and can be traced to kilometer 175 where it reaches a depth of ~ 50 km (TM1). A shallower, intermittent Moho signal (TM2) becomes evident a few 10s of km to the east before becoming better defined and more coherent by kilometer 200.

[16] The transverse component (Figure 4b) is dominated by a high amplitude signal comprising at least two parallel, oppositely polarized pulses collectively labeled AM (Anisotropic Mantle). The signal appears first at 4 s beneath station A10, is flat for 75 km and begins to dip thereafter. Its geometry is well defined until kilometer 250 whereupon it becomes unclear. The dominant early pulse, whose timing corresponds to the direct conversion from the Moho on the radial component (i.e., signals TM and $TM1$), is sharp and rich in high frequencies whereas the second pulse is more diffuse. This latter signature is characteristic of an interface defined by a more gradual variation (e.g., first-order versus zeroth-order discontinuity) in material properties [Bostock, 1999].

[17] The polarity of AM varies as a function of back-azimuth, alternating from positive to negative (red to blue). Where the layer dips and its geometry is well defined (i.e., roughly between kilometers 150 and 220), a dominantly $1-\theta$ (i.e., 360°) periodicity is observed. This behavior is illustrated in Figure 5 where data from stations UBC03, UBC04 and A12 have been aligned and sorted by back-azimuth. The polarity of the first arrival is clearly negative between 250° and 60° , weakly positive between 230° – 240° , and likely positive between 130° and 180° . Polarity reversals must evidently occur where no data are recorded between 60° and 130° , and between 240° and 250° . The precise back-azimuths at which reversals occur cannot be determined but, if the signal is strictly $1-\theta$ (i.e., polarity reversals occurring periodically every 180°), they will be restricted to the range between 60° and 65° and between 240° and 245° .

[18] Visual coherence of the signal AM can be greatly improved if polarity corrections that account for the natural periodicity of the signal, are applied to the transverse component between stations A10 and A15 (see Figure 4c). Note that the correction derived from the polarity of the signal AM along the dipping portion is also somewhat

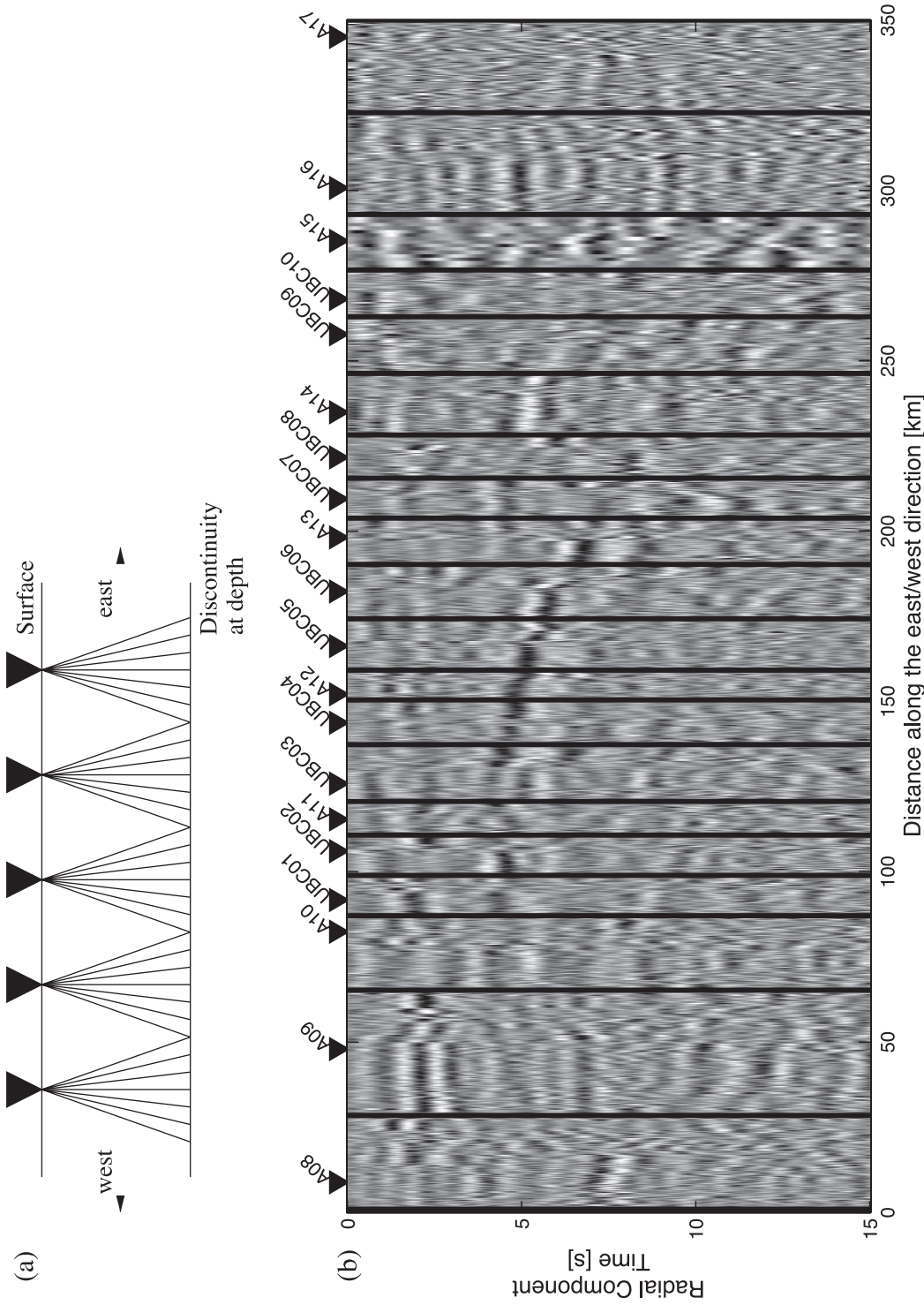


Figure 3. (a) Illustration of the approach adopted to display receiver functions along the array. The receiver functions are ordered from west to east based on (i) the geographic position of the stations, and (ii) the azimuthal sampling of events for individual stations. (b) Display format adopted for Figures 4 and 11. Black/white shading corresponds to positive/negative amplitudes, respectively. Seismic stations location are represented by reverse triangles, and projected to their location on the 61st parallel. To produce a continuous, west-east profile that accounts for variable station spacing, receiver functions for individual stations are horizontally scaled to cover that segment of the image proportional to the local interstation distance (i.e., half the sum of the distances separating a given station from its two nearest neighbors). Black vertical lines mark the plotting limits of the receiver functions for an individual station.

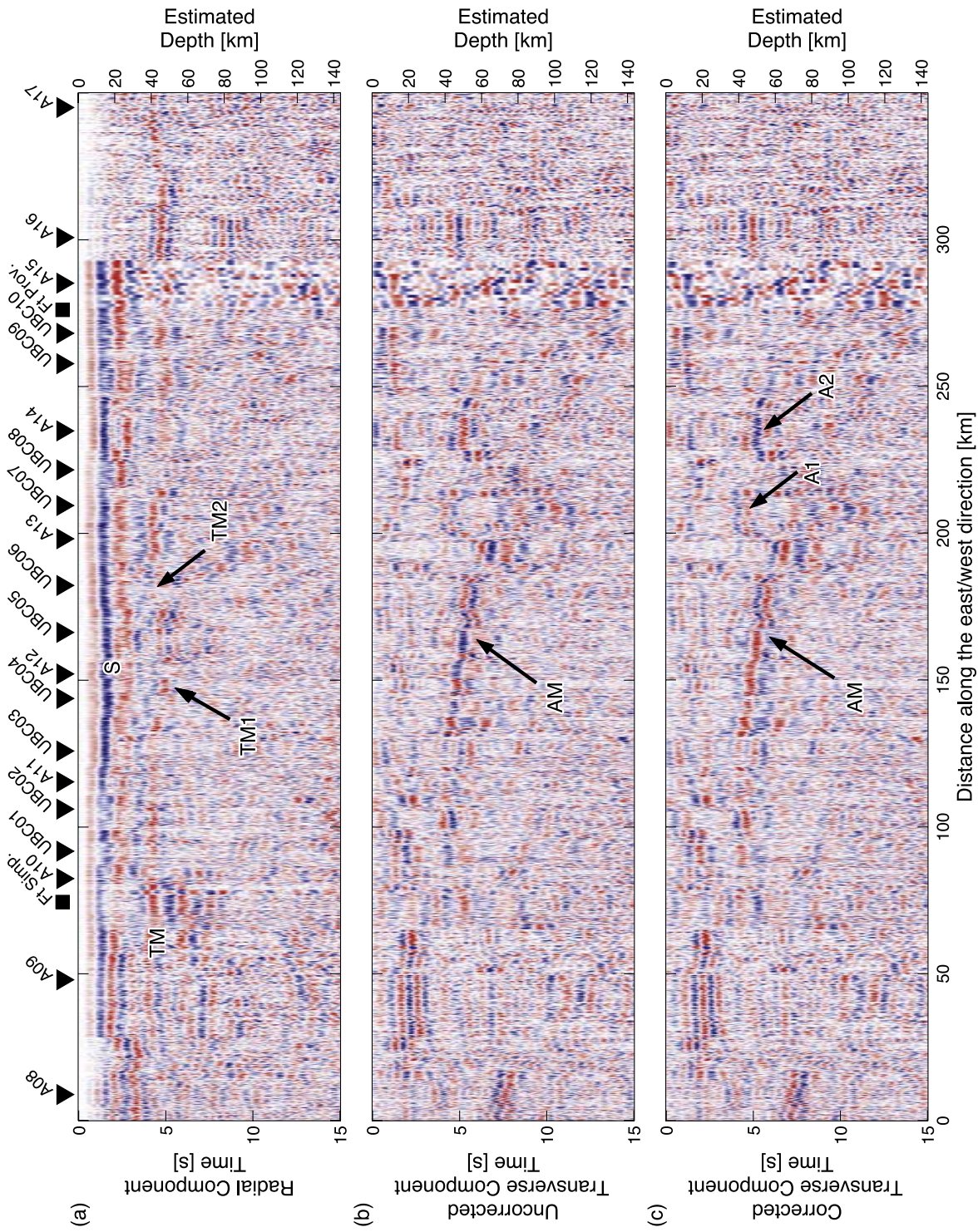


Figure 4. Radial component in (a), transverse component in (b), and polarity corrected (stations A10 through A15 only) transverse component in (c). Red/blue colors correspond to positive/negative amplitudes, respectively. In (c), the correction is applied to account for the polarity crossover in signal *AM* documented in section 5. Responses are filtered between 0.2 and 1.5 Hz.

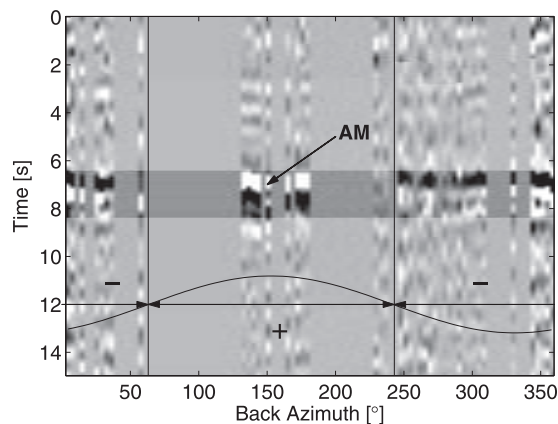


Figure 5. Transverse component azimuthal response for stations UBC03, UBC04, and A12 in the frequency band 0.2–1.5 Hz. Receiver functions are aligned along signal AM and stacked into 100 back-azimuth bins. Transparent mask was applied to the signal of interest between 6.5 and 8.5 s. Vertical lines mark estimated back-azimuth of polarity crossover. Expected $1-\theta$ amplitude variation is shown in solid line.

successful in improving its coherence over the flat portion. On the corrected transverse component, additional energy that was not readily apparent reveals further signals $A1$ and $A2$. They appear in the mantle, above the layer defined by AM and between kilometers 200 and 300. Their combined signature resembles AM in that it exhibits a similar pulse sequence and azimuthal periodicity.

6. Modeling and Numerical Simulation

[19] Estimation of elastic properties of the subsurface is an important step toward achieving an accurate interpretation of lithospheric structures from coherent signals on the receiver function images. In this section, we construct a model that succeeds in explaining the essential spatiotemporal distribution and frequency response of energy on the radial and transverse components. We draw our attention, in particular, to the layering defined by the signal AM on the transverse component.

[20] The appearance of coherent energy on the transverse-component receiver functions results from a rotation of the particle motion out of the sagittal plane (i.e., the vertical plane containing earthquake source and receiver). This rotation is the consequence of lateral heterogeneity, anisotropy or some combination thereof. In the case of AM, the signal clearly defines a dipping layer, so lateral heterogeneity must obviously contribute. There is a reason to believe, however, that anisotropy also influences the signal, in part, through the association of the continental Moho with the top of the layering AM. Note first that the absence of strong conversion from the lower (basal) interface of AM on the radial component suggests that average velocities of the layer and the underlying mantle are comparable. Moreover, the strength of AM on the transverse component does not diminish significantly as the layer dip shallows, as would be expected for a strictly isotropic layer.

6.1. Inversion

[21] To develop a model that successfully reproduces the characteristic signature of AM, most clearly expressed at stations UBC03, UBC04 and A12, we generated a suite of synthetic seismograms for plane incident P waves at a fixed slowness of 0.06 s/km and for back-azimuths varying from 0° to 360° . We used the high frequency asymptotic approach of *Frederiksen and Bostock* [2000] applied to a simple three-layer model composed of (i) a 40 km homogeneous crust (Poisson solid, $V_p = 6.6$ km/s, $\rho = 2900$ kg/m³), (ii) a homogeneous half-space mantle (Poisson solid, $V_p = 8.1$ km/s, $\rho = 3300$ kg/m³), and (iii) a dipping 10 km thick layer exhibiting hexagonal anisotropy with average mantle velocities. Hexagonal anisotropy is parametrized by the variation in P- and S-wave velocity (ΔV_p and ΔV_s), and the plunge and trend of the symmetry axis [e.g., *Sherrington et al.*, 2004, Figure 2]. Although we have specified Poisson solids for layers i) and ii), we note that S -velocity exerts the main control on amplitude of response. The dip and strike of the layer also influence the azimuthal response. On the basis of the timing of AM, we fixed the dip of the layer to 20° , ΔV_p and ΔV_s versus to $\pm 5\%$ and constrained the strike to the interval of -20° to 20° . The plunge and trend of the symmetry axis were allowed to vary from 0° to 90° , and 0° to 180° , respectively.

[22] An exploration of this reduced model space, employing a simple grid search with a sampling interval of 10° in each dimension, allowed us to obtain a model that reproduces the characteristic azimuthal signature of AM reasonably well. A solution was obtained with a model involving a strike of 0° , a plunge of 70° , and a trend of 40° as defined in Figure 6. Careful investigation revealed that no model comprising a fast symmetry axis in the plane of the dipping layer could successfully reproduce the observations. Figure 7 compares the azimuthal responses for the data and preferred model. It shows a good correspondence between observed and predicted polarities and amplitudes on both the transverse and radial components. Note, in particular, that the synthetic back-azimuthal response reproduces the dominantly $1-\theta$ pattern with polarity crossovers occurring at back-azimuths of approximately 60° and 240° .

6.2. One-Way Modeling

[23] To further validate this model and accommodate laterally varying structural dip along the array we employed a modeling code based on the wide-angle, one-way wave equation [*Thomson*, 1999] as described by *Audet et al.* [2007]. We adapted the slab geometry from *Cook et al.* [1998] and represented the structural elements as a 15 km thick layer of dipping anisotropic material, a 37 km crust and a half-space mantle with properties derived from the grid search model and identified in Table 1 (see Figure 8). The frequency dependent behavior of AM, documented in section 5, is modeled as a stack of 5 thin layers showing a decrease from strong ($\pm 5\%$) to weak anisotropy from top to bottom. The plunge of the anisotropy is rotated as the dip shallows to ensure that the fast axis maintains the same angle with respect to the plane of the dipping layer. We modeled signals $TM1$ and $TM2$ from the teleseismic Moho near the suture by a mantle wedge that displays a linear horizontal gradient in velocity from $V_p = 7$ km/s to 8.1 km/s over a distance of ~ 150 km. These velocities are broadly

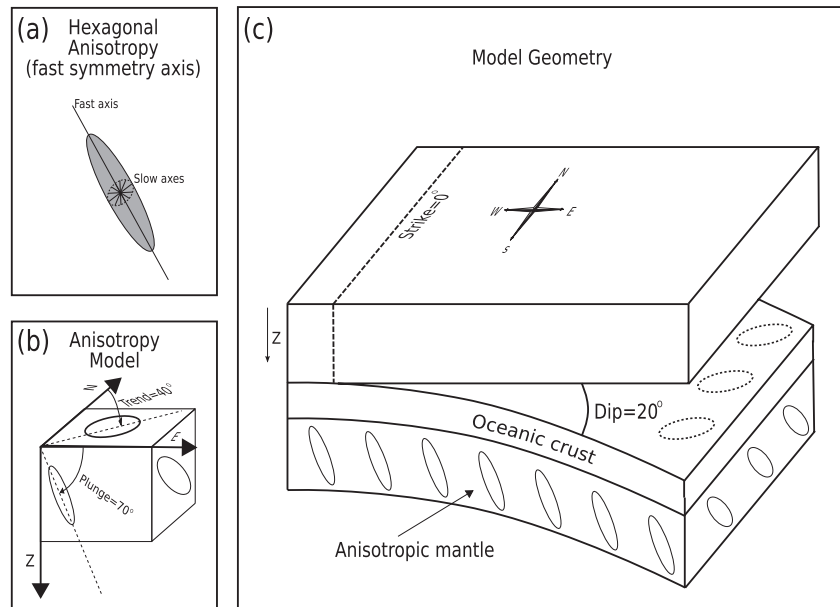


Figure 6. Cartoons showing (a) velocity ellipsoid corresponding to modeled hexagonal anisotropy with fast symmetry axis, (b) definition of trend and plunge of symmetry axis, and (c) orientation with respect to suture model.

consistent with the low-velocity mantle wedge reported by *Fernández-Viejo and Clowes [2003]* and *Fernández-Viejo et al. [2005]*.

[24] The model domain encompasses an area of 256 km × 110 km in 128 × 220 grid points for a horizontal sampling of 2 km and a vertical sampling of 500 m. Although this simplified model does not account for all the features within

the observed receiver functions it provides a good geometrical template of the suture suitable for modeling the main arrivals.

[25] To obtain results consistent with the receiver functions, we produced synthetic seismograms for a subset of 50 events from the real data-set and ordered them in like manner by geographical location, bandwidth and *P* wave

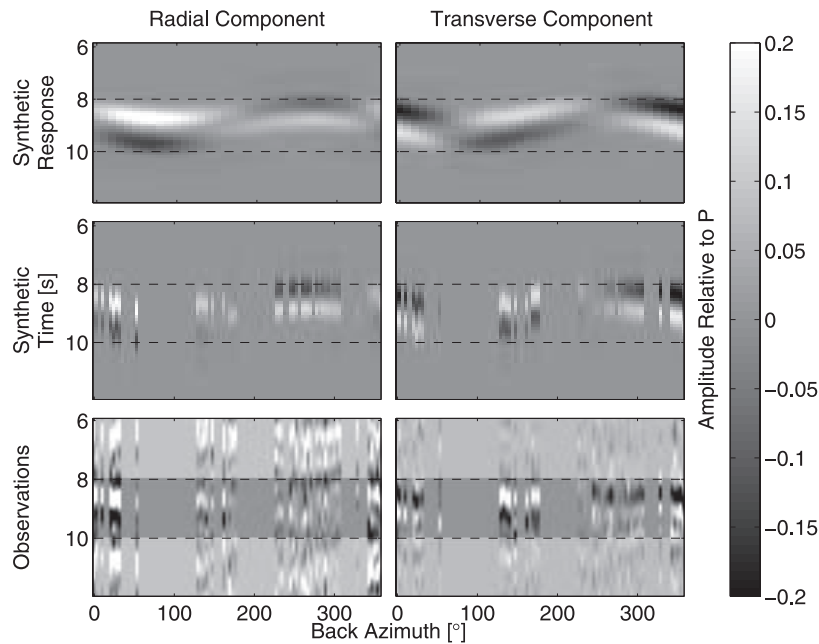


Figure 7. Radial (left) and transverse (right) back-azimuthal responses. Top row shows synthetic back-azimuthal response for incident waves with a fixed slowness of 0.06 s/km. Middle row shows synthetic impulse responses individually stacked in 3.6° back-azimuth bins for the set of slownesses and back-azimuths corresponding to the observed distribution. Bottom row shows observed receiver functions from stations UBC03, UBC04 and A12 aligned along *AM* and stacked in 3.6° back-azimuth bins.

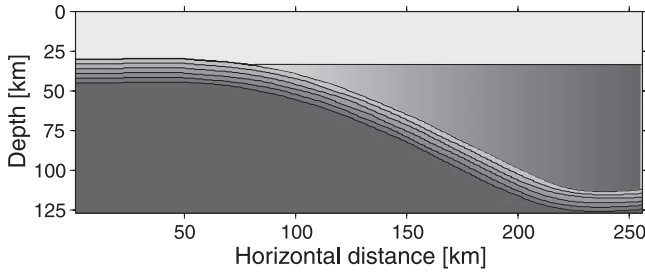


Figure 8. Subsurface model of the Wopmay Orogen showing the geometry of the dipping layer, represented as a series of 5 thin layers exhibiting a gradual linear decrease in anisotropy from top to bottom with an average mantle velocity. The maximum amplitude of hexagonal anisotropy is 5 at the top of the layer. The subcontinental wedge shows a gradual increase in velocity from 7 km/s to 8.1 km/s to the eastern edge of the model box.

slowness. The simulation results are presented in Figure 9. The synthetic radial component captures the dominant characteristics of the Moho, namely, the variable dip and the disappearance of signature at depth below the suture. The polarity is consistent with observation, being generally positive along the profile, except where the signal dips between back-azimuths of 220° and 310° . On the synthetic transverse component, the dipping layer is clearly identified and exhibits a similar frequency dependence to *AM* (see Figure 10).

7. Interpretation

[26] In this section, we place our observations in the context of several other seismic studies previously undertaken in the study area. We compare our results with the SNORCLE near-vertical reflection [Cook *et al.*, 1998; Cook and Vasudevan, 2003] and wide-angle reflection/refraction studies [Fernández-Viejo and Clowes, 2003], and teleseismic receiver function analysis from the Yellowknife array [Bostock, 1998].

7.1. SNORCLE Active Source Studies

[27] To better compare the SNORCLE near-vertical reflection profile and the leg A CANOE data, we superimpose the time migrated, coherency filtered, reflection section (dominant frequency >15 Hz) upon the radial- and transverse-component receiver functions (dominant frequency <1 Hz) in Figure 11. This is accomplished through a simple scaling between the direct *P*-to-*S* conversion time, t_{ps} , and the 2-way *P* traveltime, t_{2p} in the form

$$t_{2p} = \frac{2t_{ps}\sqrt{1 - V_p^2 p^2}}{\left(\sqrt{3 - V_p^2 p^2} - \sqrt{1 - V_p^2 p^2}\right)}, \quad (2)$$

where p is the horizontal slowness, and a Poisson solid is again assumed. For $V_p = 6$ km/s and $p = 0.06$ s/km, the scaling relation is $t_{2p} \approx 2.6 t_{ps}$.

[28] The signature of the topmost (1 km thick) sedimentary sequence *S* is manifest in different ways on the two profiles. The base of the sediments is barely visible in the

reflection data as a near-continuous reflector at $t_{2p} < 1$ s between stations A09 and A16. Its expression on the radial component receiver functions extends to significantly later times ($t_{2p} \sim 5$ s) because (i) free-surface reverberations dominate the response and are mislocated with depth as forward conversions using (2); and (ii) the teleseismic response exhibits lower frequency bandwidth, resulting in greater pulse widths.

[29] On the radial component, we observe a good correspondence between the teleseismic Moho, *TM*, and the sudden change in reflectivity with depth on the reflection profile, interpreted by Cook *et al.* [1998] as being the base of the crust. Over much of the profile, this feature remains relatively flat. At the Fort Simpson/Hottah terrane suture, however, *TM* follows the base of a dipping layer on the reflection profile over a distance of approximately 50 km. This layer is interpreted to be remnant crustal material subducted beneath the Hottah terrane during the Proterozoic. Note that the dipping signal *AM* visible on the transverse receiver function, does not coincide with the subducted crust, as inferred from the reflection profile, but rather parallels it, sharing a common interface that is the teleseismic (and reflection) Moho. An important implication of this observation is that the anisotropic layering identified on the teleseismic response represents a lid of shallowmost mantle material.

[30] East of the Fort Simpson/Hottah terrane suture (\sim kilometer 150–200 along the profile), we observe a temporary disappearance of the Moho in the depth range of 30–50 km on both the teleseismic and the near-vertical reflection profiles suggesting a reduced velocity contrast. Wide-angle reflection/refraction data indeed show high crustal and low mantle velocities along this stretch of profile [Fernández-Viejo and Clowes, 2003]. Further study by Fernández-Viejo *et al.* [2005] that combined both *P*- and *S*-wave observations yielded additional insights into the nature of the wedge. They demonstrated that the wedge region is characterized by low V_p/V_s or equivalently low Poisson's ratios, and attributed this observation to the presence of pyroxenite.

[31] Slightly to the east (kilometers 300–400 along the profile), a re-analysis of near-vertical reflection data by Cook and Vasudevan [2003] permitted the identification of synclinal mantle reflections that are discordant with the overlying Moho and which they must therefore predate. The authors suggested that these structures may have developed during the 1.8 Ga subduction event, but the lithologies responsible are difficult to constrain. It is interesting to note that the teleseismic results present evidence for structural heterogeneity within the intermediate wedge region (signals *A1* and *A2* at kilometers 200–250 in Figure 4) that appears to possess anticlinal geometry although the true geometry is difficult to ascertain given the simple imaging approach adopted here. The $1-\theta$ polarity correction applied to improve lateral coherence of *AM* on the transverse component also appears to enhance the continuity of the *A1* and *A2*

Table 1. Model Parameters

V_p , km/s	V_s , km/s	ρ , kg/m ³	Anisotropy ($\pm\%$)	Trend, deg	Plunge, deg	Strike, deg	Dip, deg
8.1	4.5	3300	5	40	70	0	20

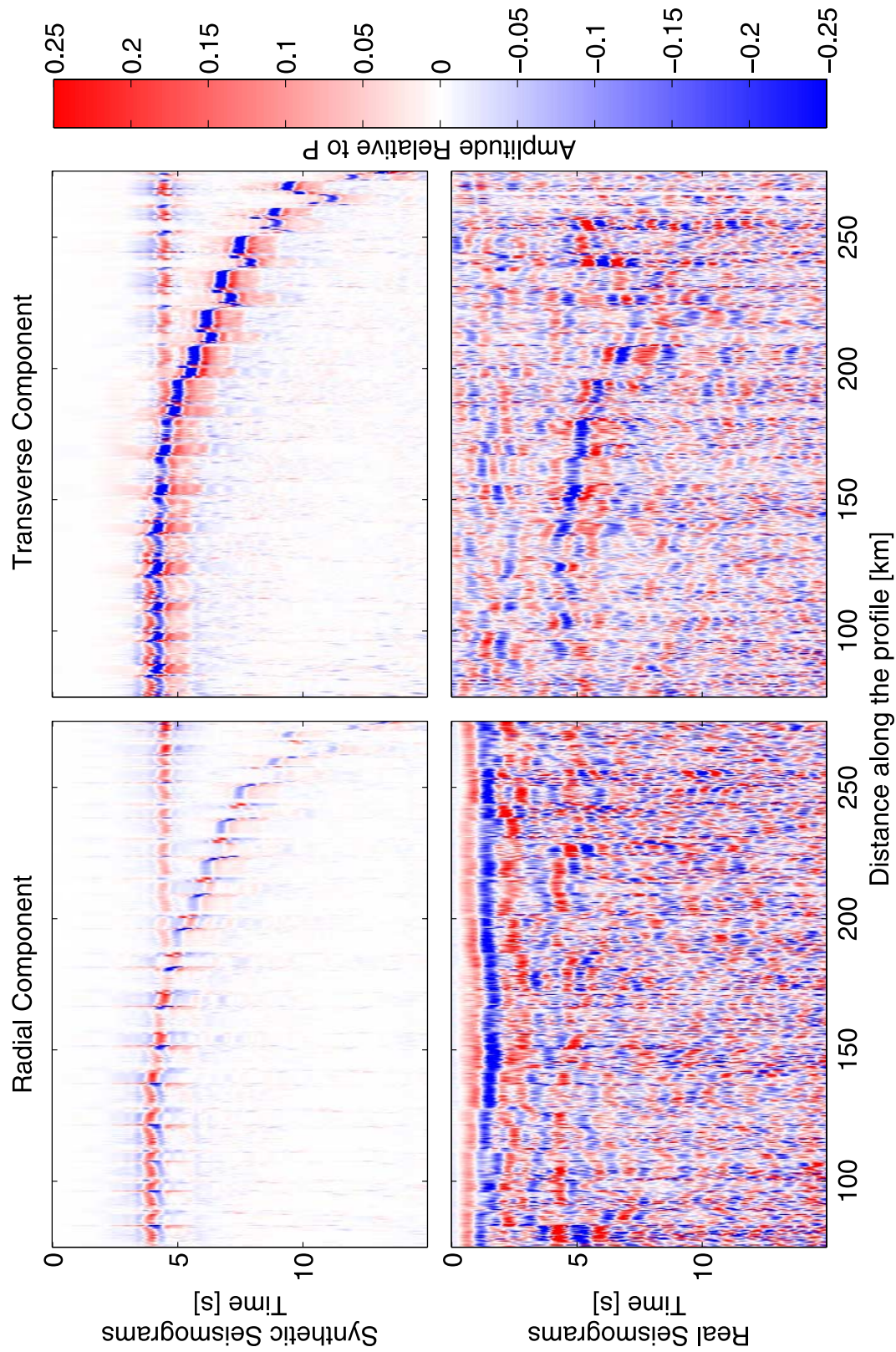


Figure 9. Comparison Synthetic (top) and observed (bottom) receiver functions for stations A10 to A15. Left panels show the radial receiver function; right panels show the transverse receiver function. The same set of slownesses and back-azimuths was used to generate the one-way synthetic data. The traces filtered between 0.2 and 1.5 Hz. Surface sediments reverberations seen on the real radial component are not modeled in the simulation. Note that the synthetics reproduce the main features of seen in the real radial and transverse component.

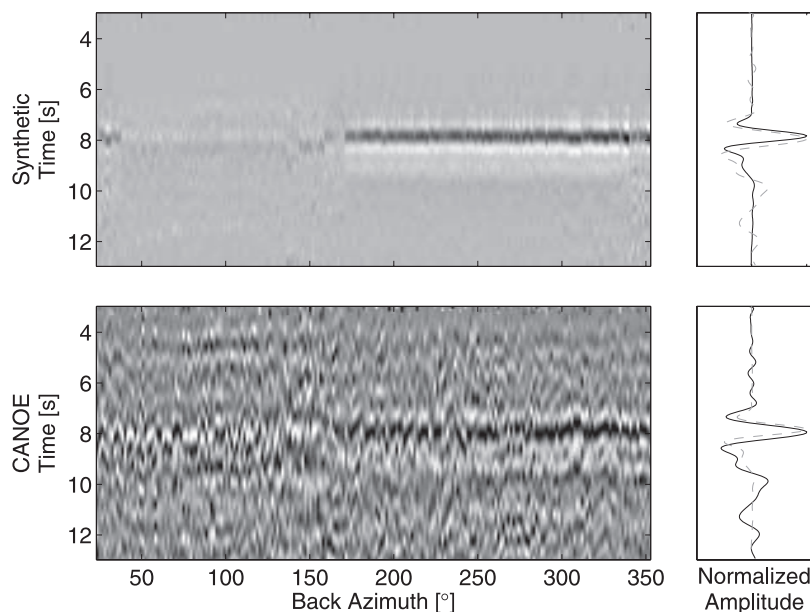


Figure 10. Comparison of synthetic (top) and real (bottom) response for stations UBC03, UBC04 and A12 for the same suite of back-azimuth and slowness. The receiver functions are aligned along AM and sorted by back azimuth. Left panels compare the azimuthal response. Right panels compare the amplitude of the stacked impulse responses.

structures and may indicate that these features are all dynamically related.

[32] East of Fort Providence, both CANOE leg A and SNORCLE reflection line 1 proceed north-east toward Yellowknife. Along this section of the Mackenzie Highway the teleseismic station distribution is sparser and the quality of the data allows only few coherent signals to be identified. Station A16 does appear to show near-horizontal layering at depths near 70 km, in particular on the radial component, that coincides with mantle reflectivity on SNORCLE line 1. As for the reflection profile, however, it is difficult to determine the relation of this structure with the main suture to the west near kilometer 150.

7.2. Comparison of CANOE and Yellowknife Array Results

[33] The Yellowknife array at the eastern terminus of leg A affords over 15 years of high quality broadband three-component data well sampled in back-azimuth and epicentral distance. As mentioned in the introduction, *Bostock* [1998] identified a series of anisotropic lithospheric mantle reflectors beneath Yellowknife: *H* at 70–80 km, *X* at 120–150 km and *L* at 170–230 km depth. He speculated that *L* could represent the continuation of the Proterozoic subducted plate observed to the west. Moreover, he interpreted the layering, and in particular *H*, as evidence for stranded oceanic crust that had developed anisotropy through a structural preferred orientation of garnet and clinopyroxene mineralogies during the process of eclogitization.

[34] The signature of *H* documented by *Bostock* [1998] and that of *AM* observed here, bear a close similarity. Figure 12 compares the two sets of aligned signals as *AM* at stations UBC03, UBC04 and A12 and *H* at YKW1, YKW2, YKW3 and YKW4. Both seismogram sections and

their summary traces exhibit a sharp earlier arrival followed by a more diffuse later pulse (note, however, that *AM* displays a lower amplitude, sharp, negative precursory pulse that is not present for *H*). Like the signal *AM*, *H* also has a counterpart on the near-vertical reflection profile in the form of a single reflection that is evident beneath the western Slave province (the Anton Terrane) including the vicinity of the Yellowknife array, at a depth of 75 km [*Cook et al.*, 1998]. It appears to be paired with a second reflection 5 km deeper over a short 10 km stretch to the east which is roughly 5 km deeper. The mantle reflection (like *H*) appears to be dominantly horizontal beneath the Slave province but shallows to the west beneath the Great Bear magmatic arc. Anisotropy is clearly manifest on *H* in polarity reversals at $\sim 180^\circ$, 270° back azimuth on the transverse component and at $\sim 320^\circ$ on the radial component, implying a dominantly $2-\theta$ symmetry. In comparing this response with that of *AM*, we corrected for the effect of slab dip in the latter feature. The corrected orientation does produce a polarity reversal near 240° back azimuth on the transverse component. The isotropic velocity contrast is, however, insufficient to produce any polarity reversal on the radial component, and the corrected symmetry axis remains at a high angle to the horizontal resulting in a complex combination of $1-\theta$, $2-\theta$ $3-\theta$ contributions.

8. Discussion and Conclusions

[35] The observations documented in the previous section bear important implications for our understanding of the structure and origin of continents. Figures 11a and 11b demonstrate that the high-frequency seismic reflection and low-frequency teleseismic signatures of fossil subduction are distinct and manifest different elastic properties. The reflection response illuminates finer-scale elasticity con-

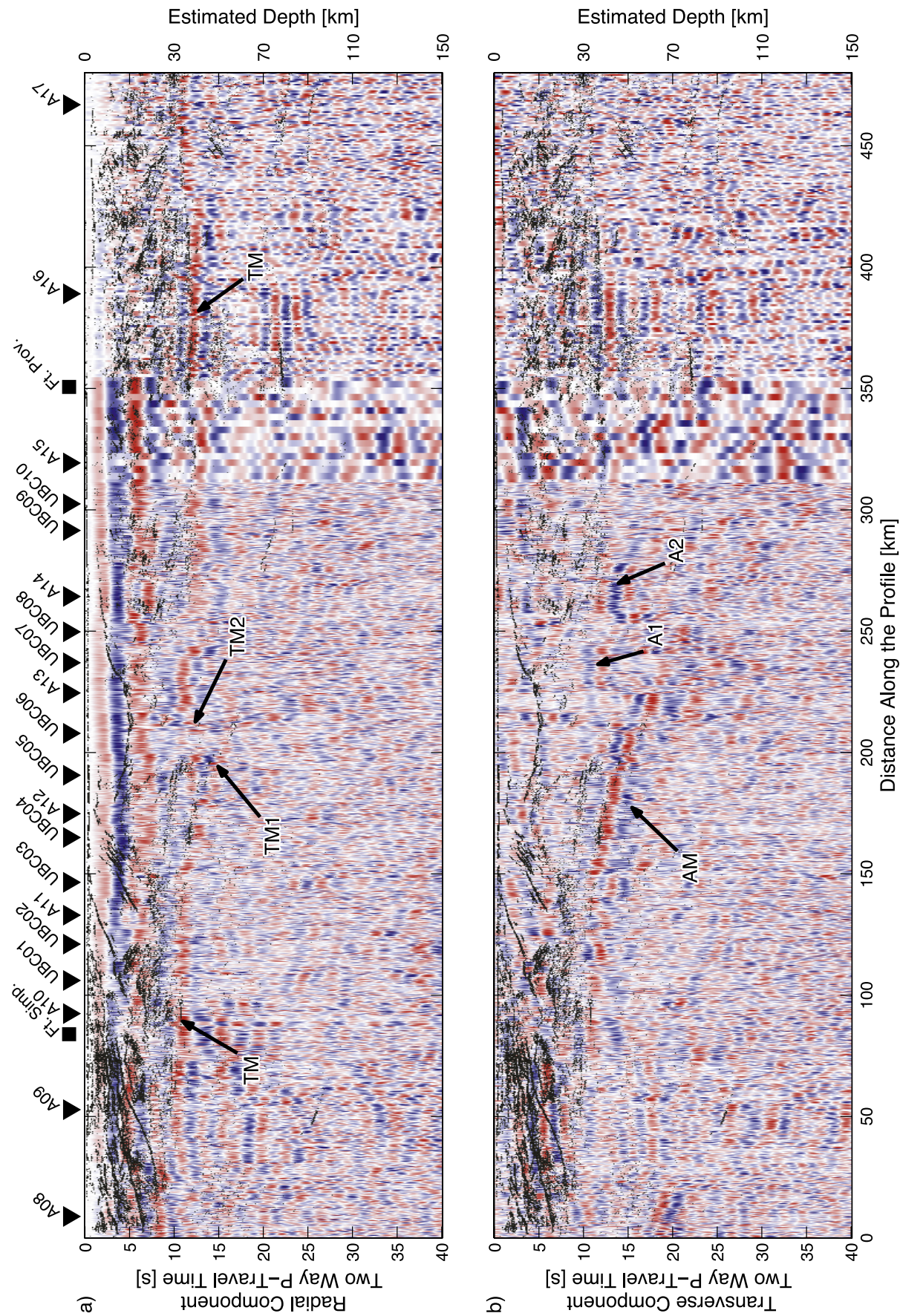


Figure 11

trasts, whereas the teleseismic signature identifies the presence of an anisotropic mantle lid within the subducted lithosphere. In this section we shall examine candidate mechanisms by which this localized (10–15 km thick) zone of mantle material, *AM*, may acquire its anisotropy, under the assumption that it represents lattice preferred orientation of olivine [Babuška and Cara, 1991]. We proceed then to examine its relation to the structure *H* observed beneath the Slave province and implications thereof for models of continental evolution.

[36] There are two obvious candidate mechanisms for the generation of *AM*, namely: (1) anisotropy has developed in situ as an immediate consequence of paleo-Proterozoic subduction/suture, or, (2) it represents an original fabric developed during genesis of the (later subducted) lithosphere at the parent mid-ocean ridge. It is also conceivable that the signature of *AM* comprises contributions from both mechanisms; in any event, stability of mantle fabric over close to 2 Ga of Earth history is implied.

[37] Studies of upper mantle peridotites from volcanic xenoliths and orogenic massifs reveal that anisotropic fabrics generally develop at high to very high temperature (>1100°C) conditions [Nicolas, 1976]. In modern-day subduction zone environments, such temperatures are unlikely to exist within the structural configuration represented by *AM*, i.e., mantle lid of subducting plate at shallow depths. However, it has been observed that lower temperature deformation of olivine can take place within 2–10 km thick shear domains that have been ascribed to transform faults [Prinzhofer and Nicolas, 1980]. It would appear reasonable, therefore, that low-temperature, localized deformation might also occur in subduction environments, especially in the near vicinity of the plate interface. The location of *AM* immediately below the former Moho and the reduction in strength of anisotropy with depth both suggest the development of simple shear strain created by stresses transmitted from the overlying plate boundary. It is necessary then to identify the factor controlling the scale of layer thickness (10–15 km). One candidate mechanism involves the eclogitization of the overlying oceanic crust. In this scenario, the ~10% volume change accompanying eclogitization within the crust creates a dimensional mismatch with underlying mantle and produces compressive stress (and consequent deformation) over a depth interval below the crust-mantle boundary that is roughly commensurate with our observations [see Kirby *et al.*, 1996, Figure 5b]. A difficulty with this interpretation is that it is inconsistent with definition of the Moho as presented on the receiver function profiles in Figure 9. Because eclogite and peridotite are characterized by comparable velocities [e.g., Christensen, 1996], we expect the transformation of crustal lithologies to eclogite to be marked by a disappearance of the Moho. The Moho

is visible to a depth of ~50 km beneath the suture (kilometer 175), setting the minimum depth of eclogitization, whereas the anisotropic mantle is well defined on the transverse component to significantly shallower levels corresponding to normal Moho depths (i.e., ~30 km depth at kilometer 100). An alternative possibility is that bending strains at the suture play a role in development of anisotropy and layer-thickness scale, although this mechanism is difficult to evaluate without more detailed modeling.

[38] Oceanic sampling and ophiolite studies suggest that dunites and olivine-rich harzburgites predominate within the oceanic lithosphere from the Moho to depths of ~25 km [Nicolas *et al.*, 1980]. These rocks are plastically deformed at the high temperatures prevailing near the ridge, with particularly large strains developing close to the Moho. Orientations of olivine and pyroxene crystals in the Bay of Islands ophiolite appear to show a systematic relation wherein orthopyroxene *c* crystallographic axes roughly correspond to the *a* axes of olivine grains [Christensen and Lundquist, 1982]. The net effect is a reduction in elastic anisotropy as the percentage of orthopyroxene within peridotite increases. These observations present an alternative interpretation for *AM*, that is, that it represent a gradient zone of increasing orthopyroxene content (with corresponding reduction in anisotropy) and decreasing deformation between the Moho and 10–15 km depth developed at a paleo-Proterozoic ridge. A combination of compositional and strain gradients may therefore define the thickness of *AM*. The steeply dipping plunge of the symmetry axis documented above may imply a slow spreading rate whereby asthenospheric flow at the ridge axis is frozen in with an intrusive, dominantly sub-vertical attitude, since the flow geometry beneath faster spreading centers is generally subhorizontal [Nicolas and Violette, 1982; Boudier and Nicolas, 1985]. A potential problem with both subduction and mid-ocean ridge mechanisms for the origin of *AM* concerns the fact that, to the best of our knowledge, there is no comparable documentation of depth-localized anisotropy within the mantle lid of subducting slabs at shallow depths in the modern context, despite a growing body of research.

[39] Notwithstanding the absence of a conclusive mechanism of formation for *AM*, its identification with paleo-subduction is important in a range of contexts. Let us first consider the Slave Province and the remarkable resemblance between the structures *AM* and *H*. If *AM* and *H* represent the same subduction episode and form part of one contiguous structure, the implication is that the bulk of mantle lithosphere beneath the western Slave province is paleo-Proterozoic (ca. 1.8 Ga) in age. However, the interpretation of these two structures as one and the same,

Figure 11. (a) Radial and (b) polarity-corrected transverse receiver functions upon which time migrated, coherency-filtered, near-vertical reflection data are superimposed with the position of the stations along the profile shown on top. The display format is slightly different from the one adopted in Figure 4 in the sense that receiver functions are projected along the profile instead of the west-east direction. To agree with two-way P traveltime of the reflection profile a simple time scaling, described in (2) was applied. An estimate of the depth based on a simplistic two layer model featuring a crust and mantle with velocity of 6 and 8 km/s, respectively is provided on the right axis. The teleseismic responses are filtered between 0.2 and 1.5 Hz. The position of the stations along the profile is shown on top.

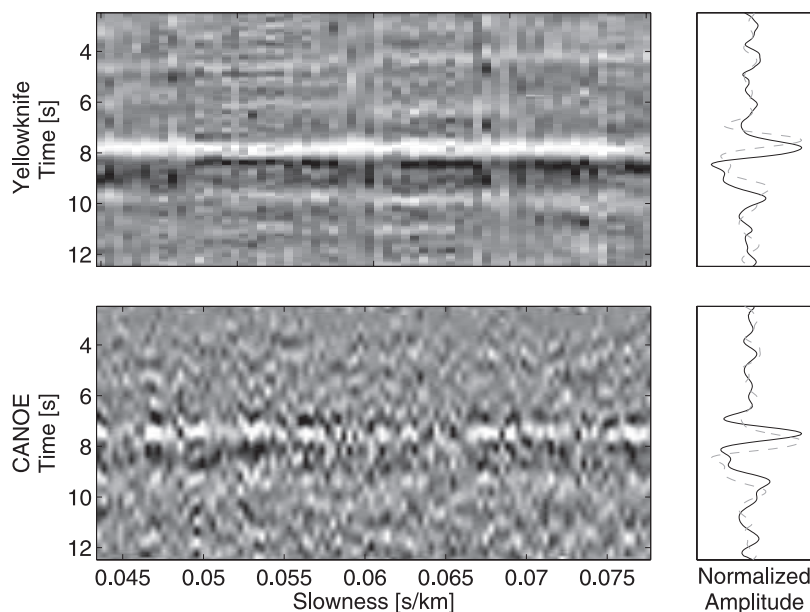


Figure 12. Comparison of receiver functions for Yellowknife array (signal H, top) and CANOE (signal AM, bottom). Impulse responses are filtered between 0.2 and 1.5 Hz and plotted between 0 and 15 s and the maximum of each trace is normalized. The left panel shows events in the back-azimuth range of 275° and 312° , sorted by horizontal slowness and moveout corrected. The right panel shows stacked receiver functions in black for Yellowknife (top) and CANOE (bottom). The gray dashed line shows the stacked receiver function for the other array, i.e., for CANOE (top) and Yellowknife (bottom).

although conceivable, would likely require shallowing toward the eastern end of the profile and stands at odds with recent evolutionary models for the Slave province based on other geophysical, geological and geochemical observations that favor development of a root by 2.6 Ga [Davis *et al.*, 2003]. We prefer therefore to interpret the similarity as due to a common, generic signature of fossil subduction as recorded in two distinct episodes of plate convergence, with *H* presumably emplaced in the late Archean and *AM* in the paleo-Proterozoic. It is unfortunate that neither the seismic reflection nor teleseismic profiles are able to definitively establish the geometric (continuous or discontinuous) relation between *AM* and *H*, *X* or *L* due to the highly variable and intermittent characteristics of the signals between the two locations.

[40] We should note that the original interpretation of Bostock [1998] that the anisotropic layering beneath YKA is the signature of subducted lithosphere is now corroborated in general, although it errs in detail because the anisotropic layering responsible for *AM* (and by inference *H*) can now clearly be identified with mantle material as opposed to eclogitized, former oceanic crust (although eclogitized crustal material presumably immediately overlies *H* as it does *AM*). This observation also renders moot another difficulty with the former interpretation, namely, that eclogite xenoliths from the Slave Province fail, for the most part, to produce a significant *S*-wave anisotropy (to which forward scattered conversions are most sensitive) as measured in the laboratory [Kopylova *et al.*, 2004].

[41] Confirmation that ancient subducted lithosphere is characterized by fine-scale (~ 10 km thick) anisotropic layering lends further credibility to the thesis that Archean cratons

were stabilized through shallow subduction processes [e.g., Vlaar, 1986; Helmstaedt and Schulze, 1989; Abbott, 1991]. Another few hundreds of km to the northeast near the center of the Slave province where the major diamond production areas are located, (D. B. Snyder, Stacked uppermost mantle layers within the Slave craton of NW Canada as defined by anisotropic seismic discontinuities, submitted to *Tectonics*, 2007) has identified similar anisotropic layering at depths near 120 km exhibiting a southeasterly dip. It would appear likely that this layering is related to one of the structures *H*, *X*, or *L* beneath YKA, and that it therefore signifies cratonic-scale lithospheric underthrusting.

[42] There are at least 3 published examples of comparable structures defined by teleseismic receiver functions on other cratons. On the Indian shield, Saul *et al.* [2000] observe a direct *P*-to-*S* conversion from the top of a similar layered structure at 90 km depth below the Dharwar craton (station Hyderabad) on both radial and transverse components. Although, the back-azimuthal distribution of events for stations in central India is limited, the strength of the signal and its moveout argue strongly for an origin in near horizontal, depth localized anisotropy. Levin and Park [2000] have modeled forward conversions from an anisotropic layer structure at 70–90 km depth beneath station RAYN on the Arabian Shield which, like *AM* and *H*, is characterized by a lower boundary that exhibits a discontinuity in material property gradient, as opposed to discontinuous material properties. Their interpretation associates the anisotropic layer with a shear zone developed in peridotitic mantle material, although they attributed its development to continental collision rather

than to the underthrusting of a subducting plate. A study of discontinuity structure beneath the Kaapvaal craton using stacked data from the portable South African experiment [Gao *et al.*, 2002] failed to find evidence for significant lithospheric layering beneath the Moho. Their analysis was based, however, on generally coarse spatial sampling and the assumption that lithospheric mantle structures are dominantly isotropic and horizontal such that possible back azimuthal variations are ignored. A separate examination of data from the subsidiary Kimberly array [Snyder *et al.*, 2003] does strongly suggest the presence of thin, anisotropic layering exhibiting variations over short distances consistent with the geographical patterns of anisotropy expressed through SKS splitting and PKP delay times [Fouch *et al.*, 2004]. We would suggest that similar structures may be found beneath other portions of Kaapvaal craton but that lateral variability in both structural geometry and anisotropic fabric preclude their detection with coarse station sampling and limited duration deployments.

[43] In summary, a growing body of evidence is pointing to the importance of shallow subduction in the stabilization of early continents. The results presented here from the Wopmay orogen in Canada's Northwest Territories provide unambiguous evidence for the signature of fossil subduction in the form of highly anisotropic, shallow-most mantle characterizing the underthrust plate. This anisotropic layering is comparable in dimension and teleseismic response to structures observed both beneath the Slave province and cratons worldwide, and which we, accordingly, infer to share a common origin. The identification of this fossil signature may provide an important diagnostic for future studies of deep continental structure and evolution.

[44] **Acknowledgments.** We gratefully acknowledge the contribution of instruments from IRIS-PASSCAL, POLARIS, Arizona State University, Georgia Institute of Technology, and the University of British Columbia. Andy Langlois provided invaluable assistance in coordination of the field effort. Discussions with Jounada Oueity and Ron Clowes helped to focus our initial analysis. We are grateful to Associate Editor Frederik Simons, Sebastian Rost and an anonymous reviewer for comments that helped improve manuscript presentation, and to Nikolas Christensen for discussion on the nature of localized mantle anisotropy. This work was financially supported by the Natural Sciences and Engineering Research Council of Canada (NSERC-Lithoprobe supporting geoscience grant CSP0006963 to MB) and National Science Foundation (grants NSF EAR-0453747 to JG, NSF EAR-0711401 to EG and NSF EAR-0003745-004 to JR).

References

- Abbott, D. (1991), The case for accretion of the tectosphere by buoyant subduction, *Geophys. Res. Lett.*, *18*(4), 585–588.
- Audet, P., M. G. Bostock, and J.-P. Mercier (2007), Teleseismic waveform modelling with a one-way wave equation, *Geophys. J. Int.*, doi:10.1111/j.1365-246X.2007.03586.x.
- Babuška, V., and M. Cara (1991), *Seismic Anisotropy in the Earth*, Kluwer, Dordrecht.
- Bostock, M. G. (1998), Mantle stratigraphy and evolution of the Slave province, *J. Geophys. Res.*, *103*(B9), 183–200.
- Bostock, M. G. (1999), Seismic waves converted from velocity gradient anomalies in the Earth's upper mantle, *Geophys. J. Int.*, *138*, 747–756.
- Boudier, F., and A. Nicolas (1985), The harzburgite and the lherzolite subtypes in ophiolitic and oceanic environments, *Earth Planet. Sci. Lett.*, *76*, 84–92.
- Bowring, S. A., and I. S. Williams (1999), Priscoan (4.00–4.03 ga) orthogneisses from northwestern Canada, *Contrib. Mineral. Petrol.*, *134*, 3–16.
- Burridge, R., M. V. D. Hoop, D. Miller, and C. Spencer (1998), Multi-parameter inversion in anisotropic elastic media, *Geophys. J. Int.*, *134*, 757–777.
- Christensen, N. I. (1996), Poisson's ratio and crustal seismology, *J. Geophys. Res.*, *101*(B2), 3139–3156.
- Christensen, N. I., and S. M. Lundquist (1982), Pyroxene orientation within the upper mantle, *Geol. Soc. Am. Bull.*, *93*, 279–288.
- Cook, F. A., and P. Erdmer (2005), Introduction to special issue on the lithoprobe Slave-northern cordillera lithospheric evolution (SNORCLE) transect, *Can. J. Earth Sci.*, *42*, 865–867, doi:10.1139/E05-067.
- Cook, F. A., and K. Vasudevan (2003), Are there relict crustal fragments beneath the moho?, *Tectonics*, *22*(3), 1026, doi:10.1029/2001TC001341.
- Cook, F. A., A. J. Van der Velden, K. W. Hall, and B. J. Roberts (1998), Tectonic delamination and subcrustal imbrication of the Precambrian lithosphere in northwestern Canada, mapped by lithoprobe, *Geology*, *26*, 839–842.
- Cook, F. A., A. J. Van der Velden, K. W. Hall, and B. J. Roberts (1999), Frozen subduction in Canada's Northwest territories: Lithoprobe deep lithospheric reflection profiling of the western Canadian shield, *Tectonics*, *18*, 1–24.
- Davis, W. J., A. G. Jones, W. Bleeker, and H. Grutter (2003), Lithosphere development in the Slave craton: A linked crustal and mantle perspective, *Lithos*, *71*, 575–589.
- Fernández-Viejo, G., and R. M. Clowes (2003), Lithospheric structure beneath the Archean Slave Province and Proterozoic Wopmay Orogen, northwestern Canada, from a lithoprobe refraction/wide-angle reflection survey, *Geophys. J. Int.*, *153*, 1–19.
- Fernández-Viejo, G., R. M. Clowes, and J. K. Welford (2005), Constraints on the composition of the crust and uppermost mantle in northwestern Canada: Vp/Vs variations along lithoprobe's SNORCLE transect, *Can. J. Earth Sci.*, *42*, 1205–1222.
- Fouch, M. J., P. G. Silver, D. R. Bell, and J. N. Lee (2004), Small-scale variations in seismic anisotropy near Kimberley, South Africa, *Geophys. J. Int.*, *764*–774, doi:10.1111/j.1365-246X.2004.02234.x.
- Frederiksen, A. W., and M. G. Bostock (2000), Modelling teleseismic waves in dipping anisotropic structures, *Geophys. J. Int.*, *141*, 401–412.
- Gaherty, J. B., and T. H. Jordan (1995), Lehmann discontinuity as the base of an anisotropic layer beneath continents, *Science*, *268*(5216), 1468–1471, doi:10.1126/science.268.5216.1468.
- Gao, S. S., P. G. Silver, and K. H. Liu (2002), Mantle discontinuities beneath southern Africa, *Geophys. Res. Lett.*, *29*(10), 1491, doi:10.1029/2001GL013834.
- Helmstaedt, H., and D. J. Schulze (1989), Southern African kimberlites and their mantle sample: Implications for Archean tectonics and lithosphere evolution, in *Kimberlites and Related Rocks*, pp. 358–368, Blackwell, Cambridge, Mass.
- Hildebrand, R. S., P. F. Hoffman, and S. A. Bowring (1987), Tectonomagmatic evolution of the 1.9 Ga Great Bear Magmatic zone, Wopmay Orogen, NW Canada, *J. Volcanol. Geotherm. Res.*, *32*, 99–118.
- Hoffman, P. F., and S. A. Bowring (1984), Short lived 1.9 Ga continental margin and its destruction, Wopmay orogen, *Geology*, *12*, 68–72.
- Isachsen, C. E., and S. A. Bowring (1994), Evolution of the Slave craton, *Geology*, *22*, 917–920.
- Kennett, B. L. N. (1991), The removal of free surface interaction from three-component seismograms, *Geophys. J. Int.*, *104*, 153–163.
- Kirby, S., E. R. Engdahl, and R. Denlinger (1996), Intermediate-depth intraslab earthquakes and arc volcanism as physical expressions of crustal and uppermost mantle metamorphism in subducting slabs, in subduction: Top to bottom, *Geophys. Monogr.*, *96*, 195–214.
- Kopylova, M. G., J. Lo, and N. I. Christensen (2004), Petrological constraints on seismic properties of the Slave mantle (Northern Canada), *Tectonophysics*, *77*, 493–510.
- Langston, C. A. (1979), Structure under mount Rainier, Washington, inferred from teleseismic body waves, *J. Geophys. Res.*, *84*(B9), 4749–4762.
- Levin, V., and J. Park (2000), Shear zones in the Proterozoic lithosphere of the Arabian Shield and the nature of the Hales discontinuity, *Tectonophysics*, *323*, 131–148.
- Nicolas, A. (1976), Flow in upper-mantle rocks: Some geophysical and geodynamic consequences, *Tectonophysics*, *32*, 93–106.
- Nicolas, A., and J. F. Violette (1982), Mantle flow at oceanic spreading centers: Models derived from ophiolites, *Tectonophysics*, *81*, 319–339.
- Nicolas, A., F. Boudier, and J. L. Bouchez (1980), Interpretation of peridotite structures from ophiolitic and oceanic environments, *Am. J. Sci.*, *280*, 192–210.
- Prinzhofer, A., and A. Nicolas (1980), The Bogota Peninsula, New Caledonia: A possible oceanic transform fault, *J. Geol.*, *88*, 387–398.
- Revenaugh, J., and T. H. Jordan (1991), Mantle layering from ScS reverberations 3. The upper mantle, *J. Geophys. Res.*, *96*, 19,781–19,810.

- Saul, J., M. R. Kumar, and D. Sarkar (2000), Lithospheric and upper mantle structure of the Indian Shield, from teleseismic receiver functions, *Geophys. Res. Lett.*, *27*(16), 2357–2360.
- Sherrington, H. F., G. Zandt, and A. W. Frederiksen (2004), Crustal fabric in the Tibetan Plateau based on waveform inversion for seismic anisotropy parameters, *J. Geophys. Res.*, *109*, B02312, doi:10.1029/2002JB002345.
- Snyder, D. B., S. Rondenay, M. G. Bostock, and G. D. Lockhart (2003), Mapping the mantle lithosphere for diamond potential using teleseismic methods, *Lithos*, *77*, 859–872.
- Thomson, C. J. (1999), The ‘gap’ between seismic ray theory and ‘full’ wavefield extrapolation, *Geophys. J. Int.*, *137*, 364–380.
- Villeneuve, M. E., R. J. Theriault, and G. M. Ross (1991), U-Pb ages and Sm-Nd signature of two subsurface granites from the Fort Simpson magnetic high, *NW Canada*, *Can. J. Earth Sci.*, *28*, 1003–1008.
- Vinnik, L. P. (1977), Detection of waves converted from *P* to *SV* in the mantle, *Phys. Earth Planet. Inter.*, *67*, 39–45.
- Vlaar, N. J. (1986), Archean global dynamics, *Geology*, *65*, 91–101.
- Wiener, N. (1949), *Extrapolation, Interpolation and Smoothing of Stationary Time Series*, Wiley, New York.
-
- P. Audet, M. G. Bostock, and J.-P. Mercier, Department of Earth and Ocean Sciences, The University of British Columbia, 6339 Stores Road, Vancouver, BC, Canada V6T 1Z4. (paudet@eos.ubc.ca; bostock@eos.ubc.ca; jmercier@eos.ubc.ca)
- J. B. Gaherty, Lamont-Doherty Earth Observatory, 61 Route 9W, Palisades, NY 10964, USA. (gaherty@ldeo.columbia.edu)
- E. J. Garnero, School of Earth and Space Exploration, Arizona State University, Box 871404, Tempe, AZ 85287-1404, USA. (garnero@asu.edu)
- J. Revenaugh, Department of Geology and Geophysics, University of Minnesota, 310 Pillsbury Drive SE, Minneapolis, MN 55455-0219, USA. (justinr@umn.edu)